Published in final edited form as:
Nat Commun. 2013 ; 4: 1393. doi:10.1038/ncomms2393.

MicroRNA-30c inhibits human breast tumour chemotherapy resistance by regulating TWF1 and IL-11

Jessica Bockhorn[1,2,*], **Rachel Dalton**[1,*], **Chika Nwachukwu**[3,4,*], **Simo Huang**[1,*], **Aleix Prat**[5,10], **Kathy Yee**[1], **Ya-Fang Chang**[1], **Dezheng Huo**[6], **Yujia Wen**[4,7], **Kaitlin E. Swanson**[1], **Tyler Qiu**[1], **Jun Lu**[8], **Seo Young Park**[6], **M. Eileen Dolan**[4,7], **Charles M. Perou**[5], **Olufunmilayo I. Olopade**[3,4], **Michael F. Clarke**[9], **Geoffrey L. Greene**[1], and **Huiping Liu**[1,9,#]

[1]The Ben May Department for Cancer Research, The University of Chicago, Chicago, IL 60637, USA

[2]Department of Biochemistry and Molecular Biology, The University of Chicago, Chicago, IL 60637, USA

[3]Center for Clinical Cancer Genetics, The University of Chicago, Chicago, IL 60637, USA

[4]Department of Medicine, The University of Chicago, Chicago, IL 60637, USA

[5]Lineberger Comprehensive Cancer Center, The University of North Carolina at Chapel Hill, Chapel Hill, NC 27599, USA

[6]Department of Health Studies, The University of Chicago, Chicago, IL 60637, USA

[7]Committee on Clinical Pharmacology and Pharmacogenomics, The University of Chicago, Chicago, IL 60637, USA

[8]Department of Genetics, Yale Stem Cell Center and Yale Cancer Center, Yale University, New Haven, CT 06520, USA

[9]The Institute for Stem Cell Biology and Regenerative Medicine, Stanford University, Stanford, California 94305, USA

Abstract

Chemotherapy resistance frequently drives tumour progression. However, the underlying molecular mechanisms are poorly characterized. Epithelial-to-mesenchymal transition (EMT) has been shown to correlate with therapy resistance, but the functional link and signalling pathways remain to be elucidated. We report here that miR-30c, a human breast tumour prognostic marker, plays a pivotal role in chemo-resistance by a direct targeting of *TWF1*, which encodes an actin-binding protein and promotes EMT. An IL-6 family member, IL-11 was identified as a secondary target of TWF1 in the miR-30c signalling pathway. Expression of miR-30c inversely correlated with TWF1 and IL-11 levels in primary breast tumours and low IL-11 correlated with relapse-free survival in breast cancer patients. Our study demonstrates that miR-30c is transcriptionally regulated by GATA3 in breast tumours. Identification of a novel miRNA-mediated pathway that

[#]Correspondence should be addressed to Huiping Liu (hliu@uchicago.edu).
[10]Present address: Translational Genomics Group, Vall d´Hebron Institute of Oncology (VHIO), Barcelona 08035, Spain.
[*]These authors contributed equally to this work

AUTHOR CONTRIBUTIONS

J.B., R.D., C.N., S.H. contributed equally to this manuscript. J.B., R.D., C.N., S.H., A.P., K.Y., Y-F.C., Y.W., K.E.S., T.Q., and H.L. designed and performed experiments and analysed data. J.L. provided the miRNA entry clones and the gateway vector backbone. S.Y.P. and D. H. performed biostatistical analyses for animal work and association studies. M.E.D., C.M.P., O.I.O., M.F.C., and G.L.G. designed the project. J.B. and H.L. wrote the manuscript. G.L.G., M.F.C., O.I.O, A.P., D.H., S.H., C.N., and M.E.D. contributed to the editing of the manuscript. G.L.G., M.F.C., O.I.O., and H.L. are equal corresponding authors on this manuscript.

regulates chemo-resistance in breast cancer will facilitate the development of novel therapeutic strategies.

Introduction

Therapy resistance, whether intrinsic or acquired, is one of the most fundamental problems in cancer and contributes to local and distant tumour recurrence and disease progression. A better understanding of the underlying molecular mechanisms will undoubtedly lead to the development of more effective therapies. Non-coding single-stranded microRNAs (miRNAs, miRs) have emerged as important epigenetic regulators of protein coding genes and aberrant miRNA expression has been found in many cancers[1]. However, the role of miRNAs in chemo-resistance remains to be characterized. In addition, the epithelial-to-mesenchymal transition (EMT) has been connected to breast cancer chemo-resistance[2,3] but the regulatory link is unknown. We therefore hypothesized that miRNAs that regulate EMT might be critical for regulating drug resistance. MiRNAs inhibit target genes primarily by degrading mRNA or by repressing translation via seed sequence-mediated imperfect, complementary binding to 3' untranslated regions (3'UTRs)[4,5]. By combining microarray analyses, miRNA target prediction algorithms, and experimental validation approaches, we sought to identify miRNA targets that regulate EMT and drug resistance in breast cancer cells.

Results

miR-30c is a prognostic biomarker in breast cancer

To identify miRNA biomarkers, we profiled primary breast tumour miRNA expression levels and performed clinicopathologic correlation analyses for breast tumours collected under IRB approved protocols at the University of Chicago Breast SPORE and in independent datasets.

Frozen primary breast tumour tissues (University of Chicago [UC] tumour set, n=46) and adjacent normal tissues (n=5) were first profiled for both gene and miRNA expression. 152 of 757 expressed miRNAs passed the filtering criteria for subsequent unsupervised hierarchical clustering (Fig. 1a; see also patient information in Supplementary Table S1). Unsupervised clustering divided the miRNAs into Cluster A and Cluster B, and these miRNAs displayed distinct expression patterns in the UC breast tumour set. Specifically, Cluster A miRNAs were up regulated in Group One tumours and Cluster B miRNAs were up regulated in Group Two tumours.

The hsa-miR-30 family segregated with the Cluster B miRNAs with high expression in Group Two patient tumours, including many known tumour-suppressor-miRs such as the let-7 family members (Fig. 1a). To determine the role of the miR-30 family members in breast cancer progression, we first examined their clinical relevance for patient survival. In an independent Oxford breast tumour dataset containing a retrospective series of 10-year follow up cases (n=210) with matched miRNA and mRNA expression arrays (GSE 22216 and GSE22220 respectively)[6], we identified miR-30c as well as miR-30a, −30a*, and −30e* as individual favourable breast cancer prognostic markers for distant relapse-free survival (DRFS) (Fig. 1b–f). The prognostic role of miR-30c is still significant even when adjusted for age, tumour size, ER status, nodal status, and histological grade (Supplementary Table S2). Furthermore, when breast tumour subtypes are classified based on the PAM50 subtype predictor[7] and the 9 Cell Line Claudin-low predictor[8], miR-30c expression is associated with breast tumour subtypes in two independent datasets (UC tumour set and Oxford tumour set[6]) (Supplementary Fig. S1a–c) and its prognostic role is subtype-dependent (Table S3).

However, the miR-30c levels were not significantly different between paired primary breast tumours and normal breast tissue adjacent to tumours (Supplementary Table S4).

By univariate analysis of a previous report, both miR-30a* and miR-30c have been shown to correlate with the benefit of tamoxifen treatment and longer progression free survival in oestrogen receptor (ER)-positive breast cancer patients[9]. However, in that study miR-30c was the only independent miRNA predictor of tamoxifen treatment response by multivariate analysis when adjusted for other clinico-phathologic factors[9]. We hypothesized that the miR-30 family, especially miR-30c, might functionally regulate therapy response in addition to having an association with treatment benefits. We therefore focused on their role in chemo-resistance regulation in breast cancer.

miR-30c regulates chemo-resistance of breast cancer cells

To test our hypothesis that miR-30c plays a role in breast tumour progression and chemo-resistance, we investigated the relevance of miR-30c to chemotherapy-induced cytotoxicity of tumour cells. Interestingly, for six breast cancer cell lines (T47D, MCF-7, MDA-MB-231, BT-20, HCC-70, and HCC-38), we observed a significant inverse correlation between miR-30c levels and cell survival in response to paclitaxel (0.1–50 nM) and doxorubicin (1–500 nM) treatments, represented as Log2-transformed expression levels and AUC (the Area Under the survival Curve, in a series of 6 treatment doses) (Fig. 2a–b, p=0.04). These correlations are more significant at the highest doses of paclitaxel (50 nM) and doxorubicin (500 nM) (Supplementary Fig. S2a–b and Table S5, p=0.0198 and 0.0191 respectively).

We further characterized the role of miR-30c in regulating chemotherapy resistance by modulating its levels in breast cancer cells. Transient transfection of miR-30c resulted in a significant decrease in survival of chemo-resistant MDA-MB-231 breast cancer cells to paclitaxel (Taxol, 0.5–10 nM) and doxorubicin (10–100 nM) at even low doses (Fig. 2c–e). Growth curve analyses suggested that increased miR-30c levels did not affect cancer cell growth (Fig. 2f). Elevated miR-30c also sensitized the drug response of a second breast cancer cell line BT-20 to paclitaxel and doxorubicin (Fig. 2g). Furthermore, DNA content analysis confirmed that miR-30c significantly increased the apoptotic sub-G1 population of these cancer cells upon paclitaxel and doxorubicin treatments (Fig. 2h).

We also examined the effects of two other individual favourable breast cancer prognostic markers in the miR-30 family, miR-30a and −30a*, on the response of MDA-MB-231 breast cancer cells to chemotherapy drugs. While ectopic miR-30a did not show any effect on doxorubicin treatment at various doses up to 200 nM, it did decrease breast cancer cell survival in response to paclitaxel at very high doses (50 nM) (Supplementary Fig. S3a–b). In addition, miR-30a* sensitized the drug response of breast cancer cells to doxorubicin (200 nM) and paclitaxel (5–50 nM) at relatively high doses (Supplementary Fig. S3a–b).

miR-30c regulates EMT and targets cytoskeleton gene TWF1

To examine the molecular mechanisms by which miR-30c regulates chemo-resistance, we investigated its target genes and focused on a few that relate to EMT regulation and cancer progression. Mammalian miRNAs regulate target genes primarily by decreasing mRNA levels[10]. Multiple computational algorithms, such as GeneSet2miRNA which identifies miRNA activities by at least four of eleven established miRNA target prediction programs[11], can predict potential interactions between genes and miRNAs. To strategically identify direct miR-30c target genes, we used global transcriptome analysis (microarray) in combination with GeneSet2miRNA and experimental validation analyses, including immunoblots, luciferase assays, and functional rescue studies.

We first performed microarray analyses of MDA-MB-231 cells that were transiently transfected either with miR-30c oligos or the scrambled control. High miR-30c levels significantly inhibited the expression levels of 291 genes in many networks and pathways, such as anti-apoptosis and cytoskeleton genes (Fig. 3a; see also Supplementary Dataset 1). Using this list, we performed online GeneSet2miRNA[11] target gene prediction analysis and narrowed the direct targets of miR-30c down to 77 potential genes, predicted by a minimum of 4 out of 11 established algorithms (Fig. 3a; see also Supplementary Table S6). Among these, the cytoskeleton genes twinfilin 1 (*TWF1*, also known as *PTK9*) and vimentin (*VIM*) were reported to regulate cell motility, drug sensitivity, and cancer progression[2,12–15].

The function of TWF1 as a regulator of drug sensitivity was previously revealed by *in vivo* RNAi screening in a lymphoma model, along with other regulators of actin dynamics, such as Rac2[12]. TWF1 is a conserved actin-binding protein with two actin depolymerizing factor homology (ADF-H) domains[16] and belongs to the ADF-H family along with ADF/cofilin, Abp1/drebrin, coactosin, and GMF[17]. It regulates diverse morphological and motile processes by both sequestering ADP-actin monomers and capping filament barbed ends[18,19]. We hypothesized that TWF1 is an important target of miR-30c by linking drug resistance to actin-based cytoskeletal organization, such as the stress fiber F-actin, an EMT marker. To address this hypothesis, we performed experimental validation analyses. Inhibition of TWF1 expression by miR-30c was confirmed in MDA-MB-231 cells by real-time PCR and western blots (Fig. 3b–c). In addition, transient transfection of an anti-miR-30c inhibitor increased TWF1 expression in these breast cancer cells (Fig. 3b). We also observed inhibitory effects of miR-30c on the EMT markers VIM and SNAI2 at protein levels compared to the scrambled miRNA control or a mock transfection control of MDA-MB-231 cells (Fig. 3c). Accordingly, elevated miR-30c promoted a round epithelial cell phenotype and reduced the stress fiber F-actin formation in MDA-MB-231 cells (Fig. 3d; large images in Supplementary Fig. S4). Further analyses and quantitative counting of stained vinculin revealed a reduction in focal adhesions, which further validated the effect of miR-30c on F-actin dynamics (Supplementary Fig. S5a–b).

We then investigated whether *TWF1* is a direct target of miR-30c. The functional interaction between miR-30 and the 3'UTR of *TWF1* was examined in luciferase assays in HEK293T cells. Compared to the scrambled control, co-transfected miR-30c suppressed the expression of the luciferase gene, which was located upstream of the wild type 3'UTR of *TWF1* (Fig. 3e; see also Supplementary Fig. S6). Mutation of all three predicted recognition sites within the 3'UTR of *TWF1* (Supplementary Fig. S6) abolished the inhibitory effect of miR-30c on luciferase activity (Fig. 3e). These data indicate that the inhibitory function of miR-30c on the target gene requires interaction with the predicted binding sites.

TWF1 is important in regulating chemo-resistance and EMT

To determine the importance of TWF1 in miR-30c–regulated drug resistance, we performed functional rescue assays by co-transfecting 3'UTR-deficient TWF1 cDNA and miR-30c in MDA-MB-231 cells. While miR-30c expression induced inhibitory effects on chemo-resistance, recombinantly expressed TWF1 (resistant to miR-30 inhibition) reversed miR-30c–mediated sensitivity of the cancer cells to doxorubicin and paclitaxel (Fig. 4a).

Equally important, knockdown of TWF1 by siRNAs copied the phenotype of high miR-30c levels by sensitizing breast tumour cells to chemotherapeutic agents doxorubicin and paclitaxel at 100nM and 10nM treatment doses respectively (Fig. 4b–c).

We further investigated the effect of TWF1 knockdown on F-actin formation in MDA-MB-231 cells. Notably, siRNAs of TWF1 dramatically inhibited F-actin organization, reduced vinculin-stained focal adhesions, and promoted the mesenchymal-to-epithelial

transition (MET) with a round cell shape (Fig. 4d; see also Supplementary Fig. S4 and S5a–b).

In addition to TWF1, VIM is another EMT-related cytoskeleton gene that is inhibited by miR-30c, as shown by microarray and western blot analyses (Fig. 3a and 3c). Overexpression of VIM reversed the drug sensitivity caused by miR-30c (Supplementary Fig. S7a), suggesting that VIM is an important target of miR-30c and may partially overlap with the effect of TWF1 in regulating drug resistance. However, knockdown of VIM is not sufficient to mimic the functions of miR-30c or increase drug sensitivity (Supplementary Fig. S7b).

IL-11 is a downstream target of miR-30c and TWF1

Interleukins (ILs) and cytokines, including IL-6 family members, have been shown to contribute to drug resistance in breast cancer and other cancers[20–23]. Based on the microarray (SAM) analysis, we observed that miR-30c suppressed expression of IL-11, one of the IL-6 family members, in breast cancer cells (Fig. 3a; see also Supplementary Dataset 1). The specific regulation of IL-11 expression by miR-30c was validated by real-time PCR analyses, demonstrating both an inhibitory effect of miR-30c oligos and a promoting effect of anti-miR-30c on IL-11 expression in MDA-MB-231 cells (Fig. 5a).

To determine the role of IL-11 in the miR-30c pathway, we also performed functional rescue studies by modulating IL-11 expression levels and functions. Overexpression of IL-11 reversed miR-30c–mediated drug sensitivity of MDA-MB-231 cells to doxorubicin and paclitaxel (Fig. 5b). In addition, we examined the effect of a neutralizing antibody to human IL-11 on drug response of MDA-MB-231 cells. The anti-IL-11 IgG added to culture media indeed copied the function of miR-30c by sensitizing cells to the doxorubicin treatment (Fig. 5c), suggesting that the secreted form of IL-11 plays a role in mediating drug resistance. Similarly, siRNA-mediated knockdown of IL-11 sensitized the response of MDA-MB-231 cells to paclitaxel (Fig. 5d).

Based on Geneset2miRNA target gene predictions, IL-11 was not on the list of predicted direct targets of miR-30 (Supplementary Table S6), suggesting that it may be a secondary target of miR-30c. We therefore explored the regulatory link between miR-30c and IL-11. Since actin affects the activity of myocardin-related transcription factors (MRTFs) and serum response factor (SRF), which regulate expression of IL-11[24], we hypothesized that TWF1, also an upstream regulator of actin dynamics, regulates IL-11 expression. We therefore examined the effect of modulated TWF1 on IL-11. As anticipated, siRNA-mediated knockdown of TWF1 inhibited IL-11 mRNA and protein expression in MDA-MB-231 cells, similar to the effect of miR-30c on IL-11 (Fig. 5e–f). These data suggest that IL-11 is an important target of TWF1 in the miR-30c signalling pathway, which regulates breast cancer chemo-resistance.

We then examined whether IL-11 also regulated F-actin formation. Indeed, knockdown of IL-11 displayed a MET phenotype very similar to that of miR-30c or knockdown of TWF1, as demonstrated both by F-actin staining and by counting of vinculin-stained focal adhesions (Fig. 5g; see also Supplementary Fig. S4 and S5a–b).

miR-30c regulates chemo-resistance in vivo

To validate the role of miR-30c as a regulator of breast tumour progression in vivo, we examined the effects of miR-30c precursor expression on chemo-resistance, using triple negative human breast tumour xenograft models generated from breast tumour-initiating cells (BTICs)[25]. To facilitate the monitoring of miR-expressing cells *in vivo*, we cloned the miR-30c precursor into a lentiviral vector (pFU-miR-30c–PGK-L2G) that co-expresses the

dual-reporter luciferase gene Luc2-eGFP (L2G) in transduced cells. Based on bioluminescence imaging following orthotopic transplantation, miR-30c precursor expression did not alter BTIC-mediated tumour growth *in vivo* (Supplementary Fig. S8a–b). At a dose of 1mg/kg, doxorubicin did not inhibit tumour growth mediated by BTICs expressing the empty L2G vector control but did significantly inhibit the growth of L2G-30c–expressing tumour cells (n=20, p≤0.00001) (Fig. 6a). This result indicates that expression of the miR-30c precursor reversed the resistance of the human breast tumour model to doxorubicin treatment *in vivo*.

To examine the functional relevance of downstream signalling pathways in vivo, we measured the expression levels of target genes in sorted breast cancer cells. Compared to vector L2G–transduced cancer cells, inhibition of TWF1 and IL-11 expression was confirmed in sorted miR-30c–expressing human breast tumour cells isolated from tumour models *in vivo* (Fig. 6b). Furthermore, the reduction of TWF1 expression at the protein level was confirmed in miR-30c–expressing tumours by immunohistochemical staining (Fig. 6c). These studies convincingly demonstrated that miR-30c regulates the downstream TWF1 and IL-11 targets and signalling pathways *in vivo*.

GATA3 regulates miR-30c expression in breast cancer

To investigate mechanisms by which miR-30 is down-regulated in Group One breast tumours, we examined possible regulation by transcription factors. JASPAR online analysis (jaspar.genereg.net)[26] identified predicted transcription factor (TF) binding sites in the putative miR-30c promoter regions, including GATA3 binding sites (Supplementary Table S7). TF-miRNA association analyses showed that GATA3 mRNA expression levels correlated with miR-30c expression levels in breast tumours (UC set, n=44, p=0.023) (Fig. 7a); a separate Oxford breast tumour dataset showed a similar correlation[6] (n=210, p<0.001) (Fig. 7a). In addition, forced expression of wild-type GATA3 induced a significant increase (8–9 fold) of miR-30c expression in GATA3-deficient MDA-MB-231 breast cancer cells (n=6, p= 1.95E-08) (Fig. 7b). These data indicate that GATA3 regulates miR-30c in breast tumours.

To determine whether GATA3 binds directly to the miR-30c promoters (30c1 and 30c2), we performed chromatin-immunoprecipitation (ChIP) assays with anti-GATA3 antibodies (Santa Cruz) using lysates of MCF-7 cells that express endogenous GATA3 and lysates of MDA-MB-231 cells that contain ectopically expressed GATA3. By ChIP and real-time PCR analyses, we observed an interaction between GATA3 with the 30c2 promoter, which contains two predicted binding elements in both cell lines and an interaction between GATA3 and the 30c1 promoter in MDA-MB-231 cells (Fig. 7c–d). These data collectively demonstrate that GATA3 transcriptionally regulates miR-30c expression in breast tumour cells.

The importance of miR-30c in a clinically relevant pathway

To validate the importance of the miR-30c signalling transduction pathway in clinical tumours, we examined the association of miR-30c with its target genes. Based on the Oxford breast tumour dataset [6] with combined mRNA and miRNA expression profiles, we observed a negative correlation between miR-30c and IL-11 expression (Fig. 8a, n=210, p=0.005). In the recently completed Breast Cancer dataset in The Cancer Genome Atlas (TCGA) [27], we also verified inverse correlations between miR-30c and TWF1 and between miR-30c and IL-11 (Supplementary Table S8, n=521, p=0.0077 and 0.0002, respectively).

In addition, relapse-free analysis with and without adjustment for nodal status, ER, grade, treatment, and tumour stage demonstrated that IL-11 is strongly associated with clinical

outcome in three independent breast tumour sets (UNC337, Oxford tumour set, and UC tumour set) for which IL-11 is a poor prognostic marker (Fig. 8b; see also Supplementary Table S9).

The above data suggest a signalling network (Fig. 8c) that links miR-30c with its upstream transcription factor GATA3 and with its downstream targets TWF1 and IL-11 and demonstrates the clinical importance of the miR-30c regulated pathway in human breast cancer.

Discussion

Our results implicate miR-30c as a phenotypic regulator of chemo-resistance. While our studies focus on the role of miR-30c as a regulator of chemotherapy response in breast tumours, miR-30 expression has been correlated with endocrine therapy resistance, which is often linked to chemotherapy resistance in advanced oestrogen receptor positive breast cancer[9].

EMT (VIM expression) has been linked with breast tumour initiating cell resistance to endocrine therapy and chemotherapy[2]. Our data demonstrate that miR-30c regulates breast cancer chemo-resistance and EMT (F-actin formation) by direct targeting of the cytoskeleton gene TWF1 as well as by indirect targeting of the cytokine IL-11. While TWF1 is known to play a significant role in regulating cancer cell chemo-resistance [12], the underlying mechanisms are not known. We have identified IL-11 as a relevant downstream target of TWF1 and demonstrated novel roles for TWF1 and IL-11 in regulating F-actin formation, an EMT marker. IL-11 belongs to the IL-6 family, which have been associated with drug sensitivity in various cancers and epithelial tissues [21,23,28]. Interestingly, TWF1 regulates the expression of IL-11 at both the mRNA and protein levels, although the detailed mechanisms remain to be elucidated. Since TWF1 is an actin-binding protein, it is likely that TWF1 regulates IL-11 through sequestering actin monomers, thereby reducing the free actin monomer pool. A reduced actin monomer pool could release actin-bound myocardin-related transcription factors (MRTFs), especially MRTFA, from trapping, thereby activating MRTFs for nuclear translocation[24,29]. Activated MRTF binds to and assists serum response factor (SRF) to trans-activate IL-11 transcription, as MRTFA−/− cells display reduced IL-11 expression levels[24].

It is of great interest to explore regulatory mechanisms of aberrantly expressed miRNAs in breast cancer. Our studies have identified GATA3 as a transcriptional regulator of miR-30c. GATA3 plays an important role in both normal mammary development and breast tumour differentiation, and its expression correlates with luminal epithelial phenotype and ER status[30–32]. MiR-30c promoter analyses also show predicted binding sites for other transcription factors (e.g. YY1 and BRCA1) that may contribute to the regulation of miR-30c expression. However, we did not observe significant correlation between YY1 and BRCA1 expression and miR-30c in the UC tumour set (data not shown). In addition to transcriptional regulation, other mechanisms can contribute to deregulated miRNA expression, such as chromatin deletions/amplifications, translocations, promoter silencing, and deficient post-transcriptional processing. In a separate study, we observed copy number variation (CNV) at chromatin regions containing miR-30c1 and miR-30c2 genes[33].

In conclusion, we have identified a novel miRNA-mediated pathway that regulates chemo-resistance in breast cancer. The components of this pathway, including GATA3, miR-30c, TWF1, and IL-11, represent attractive targets for developing new therapeutic strategies in the management of breast cancer.

Methods

All experiments were performed under the approval of the Institutional Biosafety Committee, Institutional Review Board and the Administrative Panel on Laboratory Animal Care of University of Chicago. All experiments had multiple replicates.

Breast tumour arrays and subtypes

Total RNAs were extracted from frozen tissues and cultured cells for DNA microarrays (Agilent Technologies) as described[34]. All microarray and patient clinical data are available at UNC Microarray Database (https://genome.unc.edu) and in the Gene Expression Omnibus (GEO) under accession number GSE22049 (clinical tumour/tissues) and GSE32617 (MDA-MB-231 cells). Breast tumours subtype determination was based on gene expression (PAM50 5-subtype predictor[7] and claudin-low predictor[35]) as well as immunohistochemical staining for ER, PR, HER2, EGFR, CK5/6, and CK8/18[36].

miRNA expression arrays

miRNA arrays, deposited in GEO under accession number GSE39543, were performed for frozen primary breast specimens (n=51) by Exiqon (Woburn) using the miRCURY™ Hy3™/Hy5™ power labelling kit and the miRCURY™ LNA Array (v.10.0; 757 human miRs). The expression values are log2 (Hy3/Hy5) ratios. Unsupervised hierarchical clustering of miRNAs was performed[34].

miRNA association tests

Log2-transformed miRNA levels were used in the miR-phenotype and miR-gene association tests. Expressions of miRNAs across breast tumour subtypes were compared using analysis of variance (ANOVA). P values were calculated using permutation test. For chemo-resistance association analysis, AUC (the area under the survival-concentration curve) was calculated by "$\mathrm{AUC}=\int_a^b f(x)dx$". A linear correlation test with Log 2 transformed values of AUC (or % survival) and miRNA levels were applied in the association test using R software. The correlations between genes and miRNA-30c expression were interrogated in the UC breast tumour set (n=44) and The Cancer Genome Atlas (TCGA) Breast Cancer dataset (n=521 breast samples)[27]. The normalized gene ("BRCA.exp.547.med.txt") and miRNA ("BRCA.780.precursor.txt") expression matrixes were used as provided in the TCGA portal (http://tcga-data.nci.nih.gov/docs/publications/brca_2012/). Pearson's correlation coefficients were then determined between the expression of each gene and miRNA-30c ("hsa-mir-30c.MIMAT0000244").

RNA extraction and real-time PCR

Total RNAs for array analysis were extracted using Trizol (Invitrogen) and RNAeasy mini kit (Qiagen) or RNA was precipitated with isopropanol and glycogen (Invitrogen). RT- PCR for miRNAs/genes used individual miRNA/gene Taqman primers (Applied Biosystems). RNU44 and U6 primers were used for miRNA internal controls and GAPDH for a housekeeping gene control.

Vectors and cloning

A lentiviral gateway vector pFU-attr-PGK-L2G was constructed based on pFU-L2G[25] and subcloned with miRNA precursor entry clones using LR clonase II (Invitrogen). Human TWF1 cDNA was subcloned into pDEST40 (Invitrogen) from a donor vector (ORFeome collection, the University of Chicago). Human IL-11 and GATA3 (transcript variant 2) expression vectors were purchased from Origene. Luciferase vector containing the 3'UTR of

TWF1 was obtained from Switchgear Genomics. A site directed mutagenesis kit (Stratagene) with appropriate primers (IDT) was used to mutate miR-30-binding sites.

Cell culture and transfections

Cells were maintained in DMEM (MDA-MB-231, MCF7, and Hek293T with G418) or EMEM (BT-20) with 10% fetal bovine serum (FBS) + 1% Penicillin-Streptomycin. MiRNAs (Dharmacon, negative control #4), anti-miRNAs (Exiqon, negative control A) and siRNAs (pooled) (Dharmacon) were transfected using Dharmafect (Dharmacon) at 100nM (MDA-MB-231) or 50nM (BT-20, Hek293T) and repeated on the following day. 3'UTR luciferase vectors and cDNA vectors were transfected using Fugene (Roche-Promega). For target gene rescue experiments, cells were transfected twice with cDNA vectors after two six-hour miRNA transfections.

Cell growth assays

Transfected cells were plated in phenol red free media. Next day calcein AM (Invitrogen) was added to the wells at 4 μg/μl and incubated for an hour at 37°C. Plates were read at 485/535 nM on the Wallac 1420 plate reader (Perkin Elmer).

Western blot

Cells were harvested 48 hours after transfections, lysed and sonicated in RIPA buffer. 100 μg of protein was loaded onto 4–20% gradient gels for immunoblots with antibodies to TWF1 (Genetex, GTX11439), Vimentin (Abcam, ab61780), SNAI2 (Cell signalling #9585), and β-Actin (Sigma-Aldrich, AC-15). Blots were read on Odyssey (Li-Cor).

Interleukin protein level measurement

Cell culture media were collected 36 hours post transfections. IL protein levels in the supernatants were measured using human cytokine magnetic beads and detection kit (Millipore) and read by Bioplex (BioRad).

Luciferase assay

Hek293T cells were transfected with miRNAs followed by transfection overnight with 3'UTR luciferase and control renilla vectors (Promega). Cells were lysed 48 hours later and measured using a dual luciferase kit (Promega). The luciferase signal was normalized to renilla.

Drugs, cytotoxicity and apoptosis

Paclitaxel and doxorubicin were obtained from either Chemopharmacy at the University of Chicago or Sigma. Breast cancer cells (ATCC) were treated for 72 hours with doxorubicin (0 to 1000 nM) and paclitaxel (0–10 nM). Cytotoxicity was measured using AlamarBlue (Invitrogen). Survival of cells were measured using cell titer blue (Promega) after 72 hours (MDA-MB-231) or 48 hours (BT-20) treatment. Anti-IL-11 neutralizing antibody (R&D systems) was added at 12ug/ml before treatment. One day post transfection, cells were exposed to doxorubicin (100 nM) and paclitaxel (10 nM) for 24 hours and collected for fixation in 70% ethanol and staining with propidium iodide (Sigma). DNA content was analysed using BD LSRII flow cytometer.

Immunofluorescence, histology, and microscope

Transfected cells were plated on microscope slides (Millipore) for F-actin and focal adhesion staining. Cells were fixed in 4% paraformaldehyde/PBS, washed, and stained with fluorescent phalloidin (Invitrogen F432) and SlowFade Gold antifade reagent with DAPI

(Invitrogen) or anti-vinculin (ab18058-abcam). Secondary antibody was anti-mouse Texas Red (T-862-invitrogen). Cell images were taken using Axiovert 100tv (fluorescent), Axiovert 200M (phase contrast) (Zeiss) or Olympus spinning disc confocal microscope. Focal adhesions were quantified using ImageJ software with 50 cells counted per well. Tumour and lung samples were fixed in 10% neutral buffered formalin, embedded, and sectioned. Immunohistochemical staining was performed using GFP (Cell Signaling, #2956) and hTWF1 (GeneTex, GTX11439) antibodies at Histology facility. Images were taken by Pannoramic Scan Whole Slide Scanner (CRi, Cambridge Research and Instrumentation).

Chromatin-immunoprecipitation (ChIP)

GATA3 antibodies (Santa Cruz, cat# 268 for MDA-MB-231 cells, cat#269 for MCF-7 cells) were used for ChIP according to the EZ ChIP™ Chromatin Immunoprecipitation Kit (Millipore Upstate Cell Signaling Solutions Catalog #17–371). DNA was purified using a phenol-chloroform extraction and precipitated by ethanol and glycogen. DNA was quantified using Fast SYBR Green Master Mix (Applied Biosystems). The sequences of 30c1-P1 primers: 5’ TGTGGGCTGCCTGCTGAATACAC and 5’ AGCAAGAGTGAACTGCTGCCTCCT; and 30c2–P2 primers: 5’ TTTGGAAGGGGTGGGCAGTGAAGA and 5’ ACTGACATGGTCATCCCACTTGC.

Tumour cell isolation and flow cytometer analysis

Xenograft tumours were harvested from mice with 1800 units collagenase III (Worthington) and 100 Kunitz units DNase I (Sigma) as described[25]. Dissociated tumour cells were stained with CD44-APC, H2Kd-biotin and strepavidin-PE-cy7 (BD), and DAPI in HBSS/2% FBS for further flow analysis or sorting on FacsAriaII (BD).

Lentivirus production and transduction

Second-generation packaging vectors (VPR and VSVG) [25] were used to produce miRNA precursor lentiviruses, and third-generation packaging vectors (pRSV-rev, VSVG, and pMDLg/RRE) for other lentiviruses. Viable CD44+ breast cancer cells were isolated from TN1 xenograft tumours[25] and transduced with lentiviruses at 10 or 20 multiplicities of infection (MOI 10 or 20).

Tumour transplantation and chemotherapy in mice

Tumour cells were mixed 1:1 with Matrigel (BD) and transplanted into NOD/SCID mouse mammary fad pads (both left 4^{th} and right 4^{th} mammary fat pads)[25], with a cohort of 10–20 mice per sample. Doxorubicin was injected intraperitoneally (IP) at 1mg/kg of mouse weight on day 20 and day 39 post implantation. Tumour growth was measured weekly by bioluminescence imaging.

Bioluminescence imaging

As described[25], bioluminescence images were acquired after D-luciferin (Biosynth AG) injection to mice (IP, 100 μl at 30 mg/ml per mouse) or incubation (300 μg/ml) with dissected lungs and tissues, using the IVIS Spectrum® system (Caliper Life Sciences). Data was analysed using LivingImage 4.0 Software (Caliper Life Sciences) and expressed as total photon flux.

Statistical Analysis

If not specified otherwise, a student T test was used to evaluate significance, p values and standard deviations (SD). For animal studies, tumour growth curves were analysed using a linear mixed model in R software[37] with the tumour volume (bioluminescence signals) or its fold change as a response variable. Lung metastases were analysed using Wilcoxon rank

sum test. Log transformation was taken on both tumour volume and its fold change. For predictors, time, group indicator (vector control versus miRNA overexpression, treated versus untreated), and their interactions were considered initially; then, non-significant ones were dropped later and only significant variables were kept in the final models. As two tumours were planted and observed from each mouse, mouse ID (ear tag number) was included in the model as random effect. To allow autocorrelation among the tumour size measurements from the same mouse, AR (1) (autoregressive model of order 1) was added to the error term.

Supplementary Material

Refer to Web version on PubMed Central for supplementary material.

Acknowledgments

We thank Drs. Marcus Peter, Suzanne Conzen, and Yves Lussier for suggestions and comments on the project and manuscript. We appreciate the experimental support of several core facilities, including animal facility, optical imaging core facility, flow cytometry facility, integrated microscopy core facility, DNA sequencing facility, functional genomics facility, and IHC core facility at the University of Chicago. We specifically acknowledge Ryan Duggan, James Cao, David Leclerc, Marianne Greene, Terri Li, Xin Jiang, Shirley Bond, Jaejung Kim, Hui Zheng, Andrew Gusev, Dalong Qian, Yohei Shimono, and Ravand Samaeekia for technical help and support.

This study was supported in part by The University of Chicago Women's Board (J.B.), National Institutes of Health (NIH) T90 Regenerative Medicine Training Program DK070103-05, Department of Defense Breast Cancer Research Program W81XWH-09-1-0331, Paul Calabresi K12 Award 1K12CA139160-02, NCI K99 CA160638-01, Chicago Fellows Program at the University of Chicago, and the University of Chicago Clinical and Translational Science Award (UL1 RR024999) (H.L.), The University of Chicago Cancer Research Center Pilot Fund, BSD Imaging Research Institute Pilot Research Projects Using Animal Imaging, UCMC/Northshore Collaborative Funds, a Segal Grant, and the Virginia and D. K. Ludwig Fund (G.L.G. and H.L.), funds from the Sociedad Española de Oncología Médica (SEOM) (A.P.), the Breast SPORE at University of North Carolina 5-P50-CA58223-17 (A.P. and C.M.P.), NIH R21 CA139278 and Pharmacogenetics of Anticancer Agents Research Group UO1GM61393 (M.E.D), NIH Grants U54 CA 126524 and P01 CA139490 (M.F.C.), the Breast Cancer Research Foundation (M.F.C., O.I.O., and C.M.P.), the Breast SPORE P50CA125183-05, the Doris Duke Charitable Foundation (O.I.O and C.N.), and the University of Chicago Cancer Center Support Grant CA 014599.

References

1. Lu J, et al. MicroRNA expression profiles classify human cancers. Nature. 2005; 435:834–838. [PubMed: 15944708]
2. Creighton CJ, et al. Residual breast cancers after conventional therapy display mesenchymal as well as tumor-initiating features. Proceedings of the National Academy of Sciences of the United States of America. 2009; 106:13820–13825. [PubMed: 19666588]
3. Singh A, Settleman J. EMT, cancer stem cells and drug resistance: an emerging axis of evil in the war on cancer. Oncogene. 2010; 29:4741–4751. [PubMed: 20531305]
4. Bartel DP. MicroRNAs: genomics, biogenesis, mechanism, and function. Cell. 2004; 116:281–297. [PubMed: 14744438]
5. Fabian MR, Sonenberg N, Filipowicz W. Regulation of mRNA translation and stability by microRNAs. Annu Rev Biochem. 2010; 79:351–379. [PubMed: 20533884]
6. Buffa FM, et al. microRNA-Associated Progression Pathways and Potential Therapeutic Targets Identified by Integrated mRNA and microRNA Expression Profiling in Breast Cancer. Cancer research. 2011; 71:5635–5645. [PubMed: 21737487]
7. Parker JS, et al. Supervised risk predictor of breast cancer based on intrinsic subtypes. J Clin Oncol. 2009; 27:1160–1167. [PubMed: 19204204]
8. Prat A, et al. Phenotypic and molecular characterization of the claudin-low intrinsic subtype of breast cancer. Breast Cancer Res. 2010; 12:R68. [PubMed: 20813035]

9. Rodriguez-Gonzalez FG, et al. MicroRNA-30c expression level is an independent predictor of clinical benefit of endocrine therapy in advanced estrogen receptor positive breast cancer. Breast Cancer Res Treat. 2011; 127:43–51. [PubMed: 20490652]
10. Guo H, Ingolia NT, Weissman JS, Bartel DP. Mammalian microRNAs predominantly act to decrease target mRNA levels. Nature. 2010; 466:835–840. [PubMed: 20703300]
11. Antonov AV, Dietmann S, Wong P, Lutter D, Mewes HW. GeneSet2miRNA: finding the signature of cooperative miRNA activities in the gene lists. Nucleic Acids Res. 2009; 37:W323–W328. [PubMed: 19420064]
12. Meacham CE, Ho EE, Dubrovsky E, Gertler FB, Hemann MT. In vivo RNAi screening identifies regulators of actin dynamics as key determinants of lymphoma progression. Nat Genet. 2009; 41:1133–1137. [PubMed: 19783987]
13. Palmgren S, Vartiainen M, Lappalainen P. Twinfilin, a molecular mailman for actin monomers. J Cell Sci. 2002; 115:881–886. [PubMed: 11870207]
14. Kokkinos MI, et al. Vimentin and epithelial-mesenchymal transition in human breast cancer--observations in vitro and in vivo. Cells, tissues, organs. 2007; 185:191–203. [PubMed: 17587825]
15. Sommers CL, et al. Loss of epithelial markers and acquisition of vimentin expression in adriamycin- and vinblastine-resistant human breast cancer cell lines. Cancer research. 1992; 52:5190–5197. [PubMed: 1382837]
16. Ojala PJ, et al. The two ADF-H domains of twinfilin play functionally distinct roles in interactions with actin monomers. Mol Biol Cell. 2002; 13:3811–3821. [PubMed: 12429826]
17. Poukkula M, Kremneva E, Serlachius M, Lappalainen P. Actin-depolymerizing factor homology domain: a conserved fold performing diverse roles in cytoskeletal dynamics. Cytoskeleton (Hoboken). 2011; 68:471–490. [PubMed: 21850706]
18. Helfer E, et al. Mammalian twinfilin sequesters ADP-G-actin and caps filament barbed ends: implications in motility. EMBO J. 2006; 25:1184–1195. [PubMed: 16511569]
19. Paavilainen VO, et al. Structural basis and evolutionary origin of actin filament capping by twinfilin. Proc Natl Acad Sci U S A. 2007; 104:3113–3118. [PubMed: 17360616]
20. Pu YS, et al. Interleukin-6 is responsible for drug resistance and anti-apoptotic effects in prostatic cancer cells. Prostate. 2004; 60:120–129. [PubMed: 15162378]
21. Duan Z, Feller AJ, Penson RT, Chabner BA, Seiden MV. Discovery of differentially expressed genes associated with paclitaxel resistance using cDNA array technology: analysis of interleukin (IL) 6, IL-8, and monocyte chemotactic protein 1 in the paclitaxel-resistant phenotype. Clin Cancer Res. 1999; 5:3445–3453. [PubMed: 10589757]
22. Vega MI, et al. Rituximab inhibits p38 MAPK activity in 2F7 B NHL and decreases IL-10 transcription: pivotal role of p38 MAPK in drug resistance. Oncogene. 2004; 23:3530–3540. [PubMed: 15077178]
23. Putoczki T, Ernst M. More than a sidekick: the IL-6 family cytokine IL-11 links inflammation to cancer. J Leukoc Biol. 2010; 88:1109–1117. [PubMed: 20610798]
24. Medjkane S, Perez-Sanchez C, Gaggioli C, Sahai E, Treisman R. Myocardin-related transcription factors and SRF are required for cytoskeletal dynamics and experimental metastasis. Nat Cell Biol. 2009; 11:257–268. [PubMed: 19198601]
25. Liu H, et al. Cancer stem cells from human breast tumors are involved in spontaneous metastases in orthotopic mouse models. Proc Natl Acad Sci U S A. 2010; 107:18115–18120. [PubMed: 20921380]
26. Wasserman WW, Sandelin A. Applied bioinformatics for the identification of regulatory elements. Nature reviews. 2004; 5:276–287.
27. Comprehensive molecular portraits of human breast tumours. Nature. 2012; 490:61–70. [PubMed: 23000897]
28. Gibson RJ, et al. Effect of interleukin-11 on ameliorating intestinal damage after methotrexate treatment of breast cancer in rats. Dig Dis Sci. 2002; 47:2751–2757. [PubMed: 12498296]
29. Posern G, Treisman R. Actin' together: serum response factor, its cofactors and the link to signal transduction. Trends Cell Biol. 2006; 16:588–596. [PubMed: 17035020]
30. Asselin-Labat ML, et al. Gata-3 is an essential regulator of mammary-gland morphogenesis and luminal-cell differentiation. Nat Cell Biol. 2007; 9:201–209. [PubMed: 17187062]

31. Hoch RV, Thompson DA, Baker RJ, Weigel RJ. GATA-3 is expressed in association with estrogen receptor in breast cancer. International journal of cancer. 1999; 84:122–128.

32. Kouros-Mehr H, Slorach EM, Sternlicht MD, Werb Z. GATA-3 maintains the differentiation of the luminal cell fate in the mammary gland. Cell. 2006; 127:1041–1055. [PubMed: 17129787]

33. Nwachukwu C LH, Bockhorn J, Prat A, Clark-Raymond A, Huang S, Han Y-J, Huo D, Greene G, Perou CM, Xu J, Olopade OI. MicroRNAs down-regulated in primary basal-like breast cancers. submitted. 2012

34. Hu Z, et al. The molecular portraits of breast tumors are conserved across microarray platforms. BMC Genomics. 2006; 7:96. [PubMed: 16643655]

35. Prat A, et al. Phenotypic and molecular characterization of the claudin-low intrinsic subtype of breast cancer. Breast Cancer Res. 2011; 12:R68. [PubMed: 20813035]

36. Huo D, et al. Population differences in breast cancer: survey in indigenous African women reveals over-representation of triple-negative breast cancer. J Clin Oncol. 2009; 27:4515–4521. [PubMed: 19704069]

37. Team, RDC. R Foundation for Statistical Computing. Austria: Vienna; 2011. R: A language and environment for statistical computing.

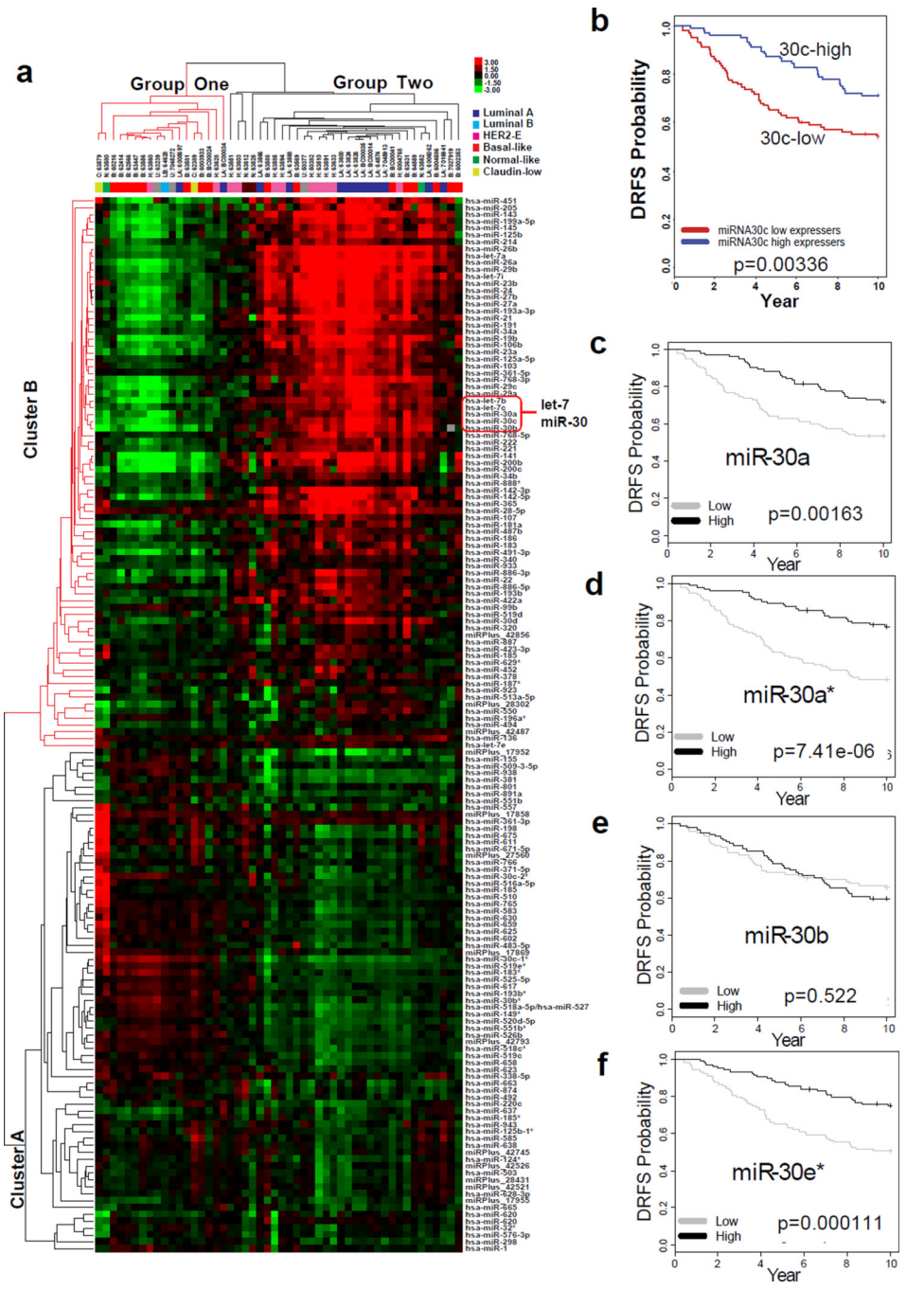

Figure 1. miRNA profiling of human breast tumours

a. Heat map diagram with two-way unsupervised hierarchical clustering of miRNAs and breast tumour samples. Each row represents a miRNA and each column represents a sample. The miRNA clustering tree is shown on the left (Cluster A and B), and the sample clustering tree appears at the top (Group One and Two). The colour scale shown in the map illustrates the relative expression level of a miRNA across all samples: red represents an expression level above the mean; green represents expression lower than the mean. Black means median expression. Levels of 152 miRNAs passed filtering and shown from 51 frozen human breast samples (46 breast tumours and 5 normal mammary tissues). NL-normal-like,

LA-luminal A, LB-luminal B, B-basal-like, H-HER2-enriched, C-claudin-low, U-undetermined, N-normal (normal breast tissue adjacent to tumours).

b–f. Kaplan-Meier plots of distant relapse-free survival (DRFS) based on the expression of miR-30 family members (30c, 30a, 30a*, 30b, and 30e*). Associations of miR-30 members with DRFS were analysed with GSE22216 breast cancer data set (n=210) deposited by Buffa et al[6]. To define low (blue) and high (red) expressers, samples were ranked ordered based on miRNA30 expression and the top 50% samples were defined as high expressers. Log rank test p values are shown.

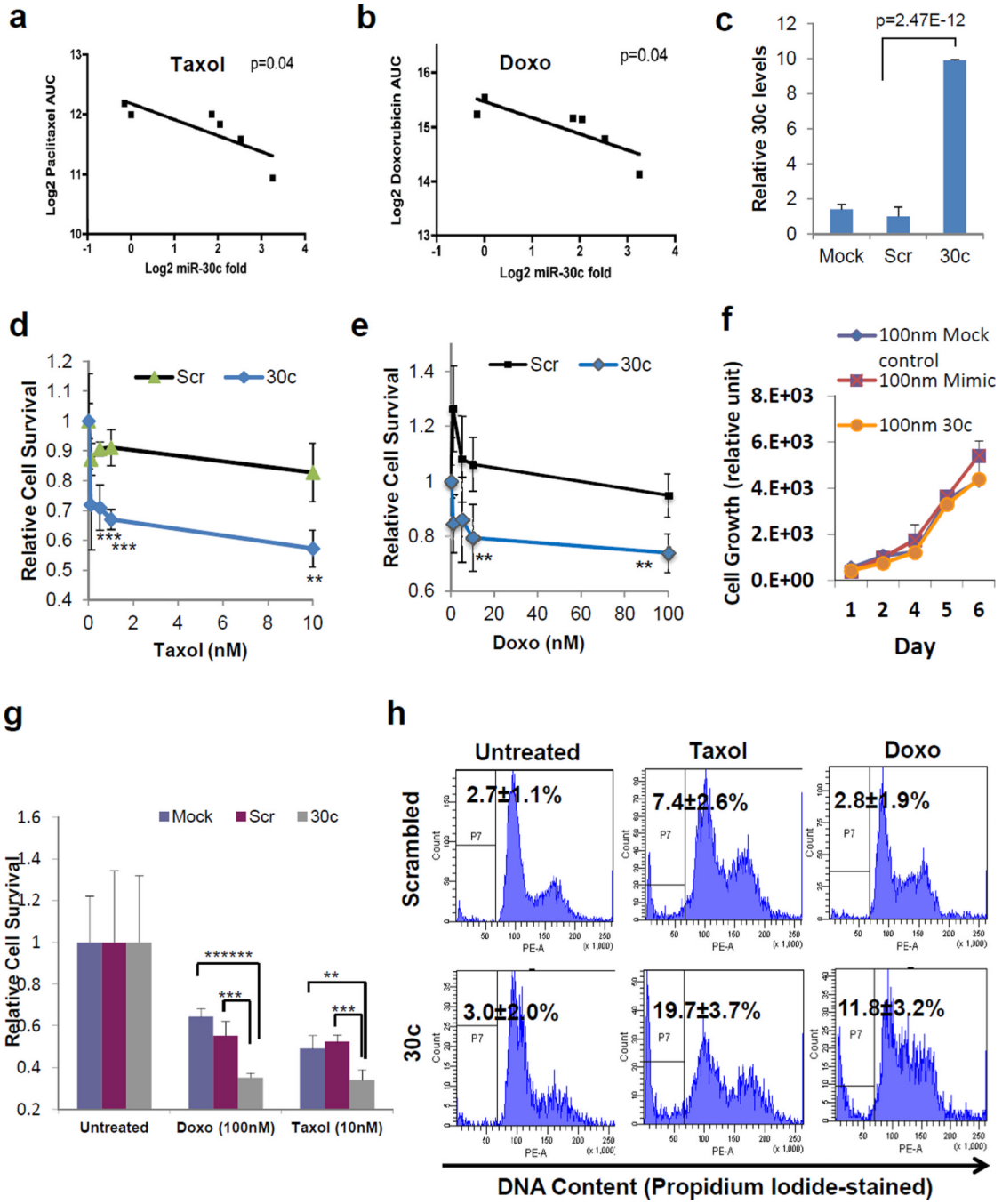

Figure 2. miR-30c corresponds to and regulates chemo-resistance of breast cancer cells

a–b. Association of Log2-transformed miR-30c expression (fold) with the survival (log2-transformed AUC) of breast cancer cell lines (n=6, T47D, MCF-7, MDA-MB-231, BT20, HCC70, and HCC38) in response to paclitaxel (Taxol) at 0.1–50 nM (**a**) and doxorubicin at 1–500 nM (**b**). A linear correlation test p=0.04 for both association studies.

c. Log2-transformed expression levels of miR-30c in MDA-MB-231 cells 48hrs after oligo transfections, measured by real-time PCR. P=2.47E-12 by a T test (n=3). Error bars represent the standard deviation (SD) of the mean.

d–e. Cell survival of MDA-MB-231 cells after transient transfection of scrambled control and mature miR-30c oligos, upon 72-hr exposure to different doses of paclitaxel (Taxol, **d**) and doxorubicin (Doxo, **e**). T test p=0.00022 (0.5 nM), 0.00014 (1.0 nM), and 0.00191 (10 nM) for Taxol treatment, and p=0.00802 (10 nM) and 0.00212 (100 nM) for Doxo treatment, comparing 30c samples to Scr samples (n=6). Error bars: SD.

f. No significant effect of transient transfection of miR-30c on the growth rate of MDA-MD-231 cells, compared to a mock transfection control and a scrambled RNA mimic control. Error bars: SD.

g. miR-30c sensitized the drug response of BT-20 breast cancer cells to 48 hr-treatment of doxorubicin (100nM) and paclitaxel (Taxol, 10nM). When comparing 30c to controls, T test p=5.52E-07 (mock) and 0.0003 (Scr) for Doxo, p=0.0066 (mock) and 0.0009 (Scr) for Taxol (n=5). Error bars: SD.

h. Representative flow profiles of BT20 breast cancer cell DNA content upon 24-hr treatment of paclitaxel (Taxol, 10nM) or doxorubicin (Doxo, 100nM). The gated sub-G1 population represents early apoptotic cells. SD values of the mean are shown.

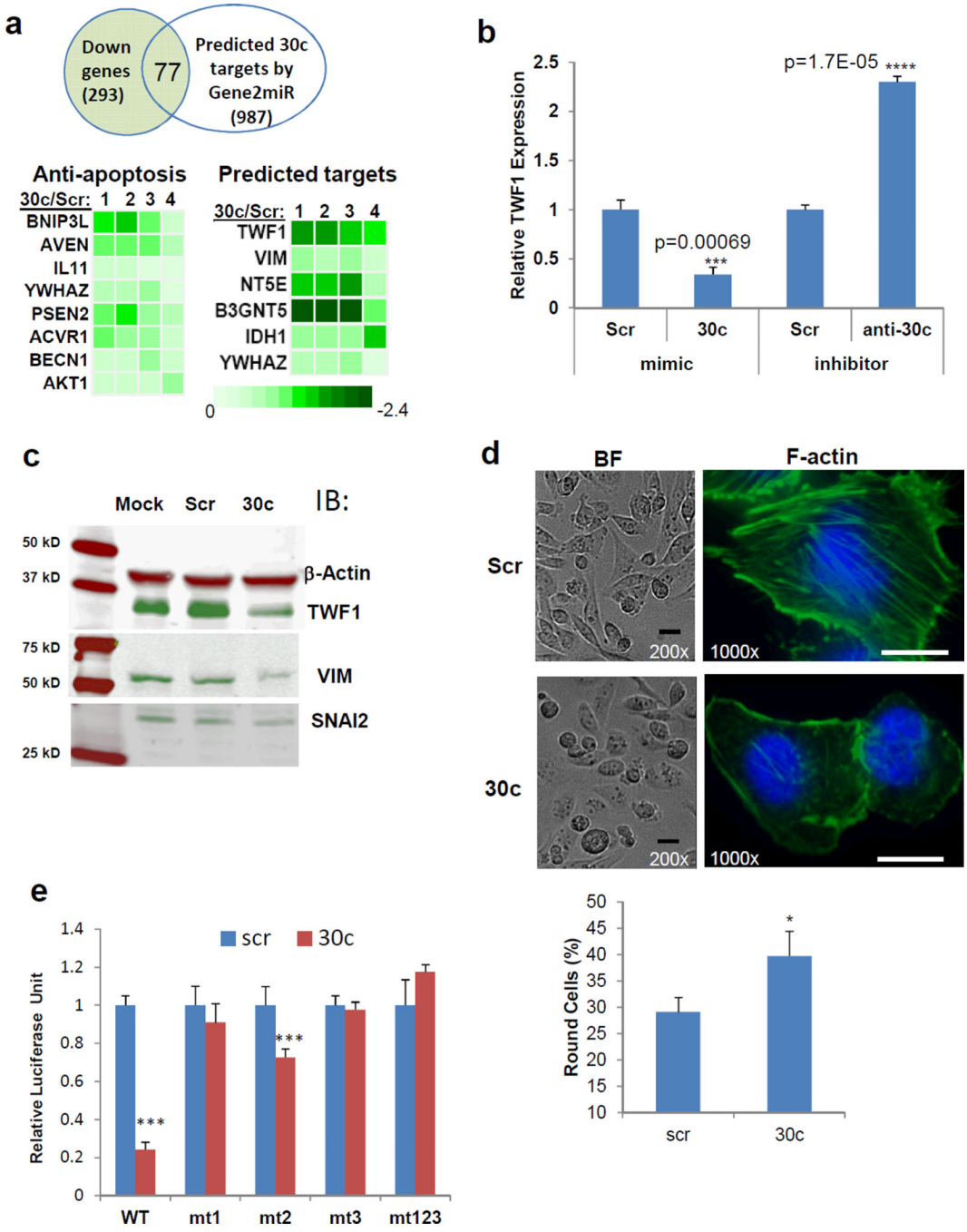

Figure 3. miR-30c regulates EMT and directly targets TWF1

a. Genes suppressed by miR-30c in breast cancer cells. Top panel: Left circle shows the microarray data of 293 genes significantly inhibited by miR-30c in MDA-MB-231 cells (See Suppl. Table 2). The right circle indicates the genes predicted as direct targets of miR-30c by Geneset2miR (by ≥4 of 11 algorithms) and overlapped genes are 77 (Suppl. Table 3). Bottom left panel: Heatmap for 8 anti-apoptotic genes inhibited by miR-30c. Bottom right panel: Heatmap for predicted direct targets, down-regulated in miR-30c–transfected cells. Green boxes are color-coded based on log2-transformed expression reduction levels for 4 pairs of 30c/scrambled microarray comparisons.

b. Expression levels of TWF1 (measured by real-time PCR) upon transfection of miR-30c or the anti-miR-30c inhibitors into MDA-MB-231 cells. T test p values are shown (n=3). Error bars: SD.

c. Immunoblots of TWF1 (green band, top panel), VIM (green band, middle panel), SNAI2 (green band, bottom panel) and beta-actin (red band, top panel) with protein lysates of MDA-MB-231 cells 36hrs after transfections of Mock control, scrambled (Scr), and oligo miRNA-30c respectively.

d. Effects of miR-30c on cell morphology and F-actin. Top panels: images of MDA-MB-231 cells after miR-30c transfections. Top left panels: bright field (BF) images of cells (200x, black scale bars=10μm). Top right panels: fluorescent images (1000x, white scale bars=5μm) with F-actin staining (green) and DAPI staining of DNA (blue). Bottom histogram: percentage of round cells counted in two groups, scrambled and 30c–transfected cells (n=4, counting 4 replicates of 100–150 cells). Cells were harvested 36hrs after transfections of scramble control (top) or miR-30c oligos (bottom). T test p=0.043. Error bars: SD.

e. Luciferase activity assays of Hek293T cells co-transfected with miR-30c (or scrambled control, scr) and the luciferase vector containing wildtype (WT) or mutated (mt) 3'UTR of TWF1. Mt1, 2, 3 are mutants with G/C converted to T in individual predicted binding site 1, 2, or 3, and mt123 contains all three mutated sites (see Supplementary Fig. S3). T test p=0.0001 for WT or mt2, comparing 30c to scr control (n=5). Error bars: SD.

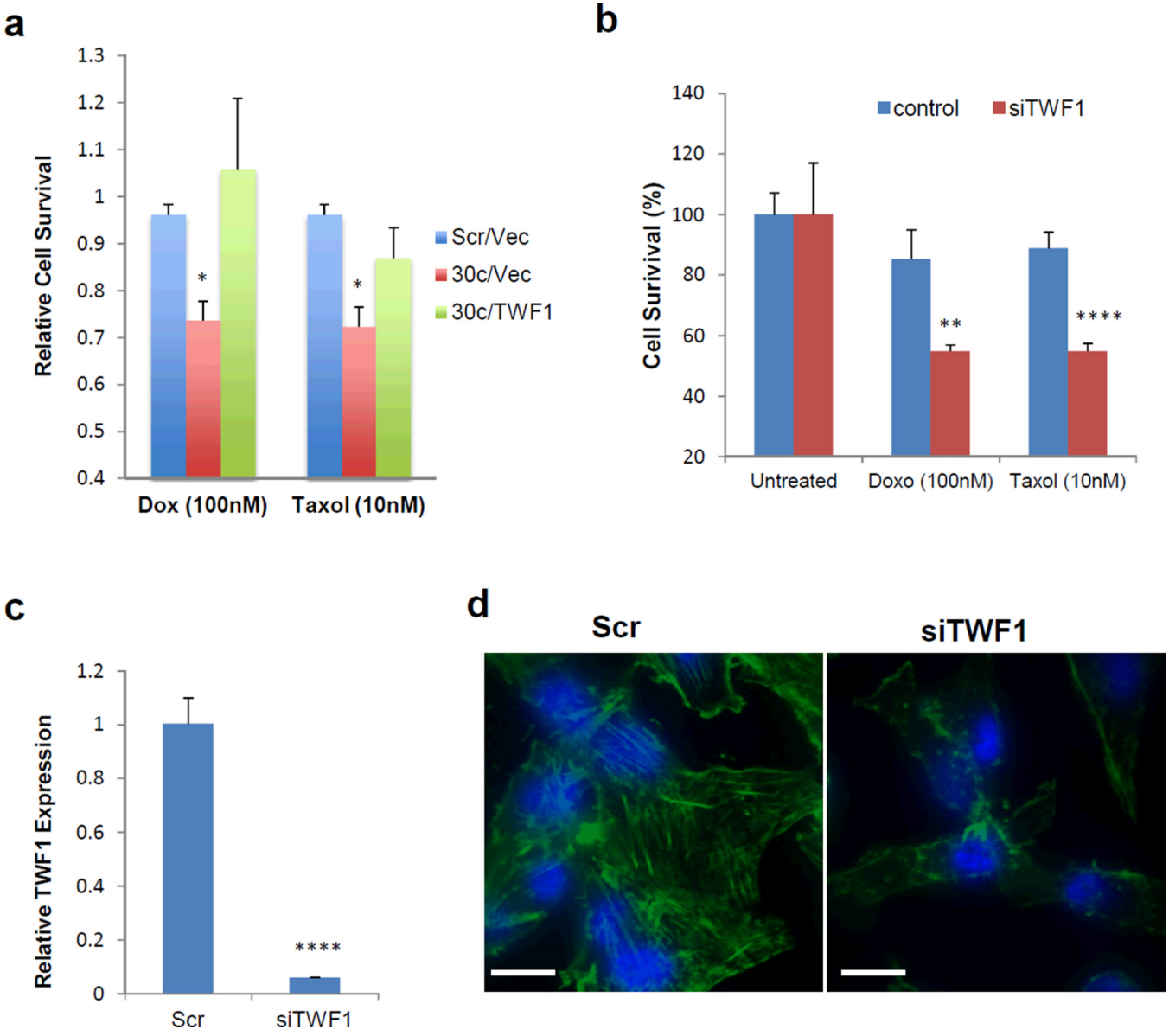

Figure 4. TWF1 is required for miR-30c functions

a. Overexpression of TWF1 reversed the chemo-response sensitized by miR-30c in MDA-MB-231 cells upon doxorubicin (Doxo) or paclitaxel (Taxol) treatments. T test p=0.01 (Doxo) and 0.02 (Taxol), when comparing 30c/Vec to 30c/TWF1 (n=5). Error bars: SD.

b. Knockdown of TWF1 by a transient transfection of siRNAs of TWF1 (siTWF1) mimicked the miR-30 overexpression to enhance the cytotoxicity of doxorubicin (Doxo) and paclitaxel (Taxol) in MDA-MB-231 cells. **p=0.0049, ****p=4.77E-05 (n=5) by a T test. Error bars: SD.

c. Relative expression levels of TWF1 upon siRNA transfections, measured by real-time PCR (BD Taqman assays). T test p= 7.31E-05 (n=3). Error bars: SD.

d. Images of F-actin staining of MDA-MB-231 cells inhibited by siTWF1 knockdowns, compared to scrambled cont-rol (Scr) (1000x, green for F-actin staining and blue for DAPI staining), white scale bars=5μm. Cells were harvested 36hrs after transfections.

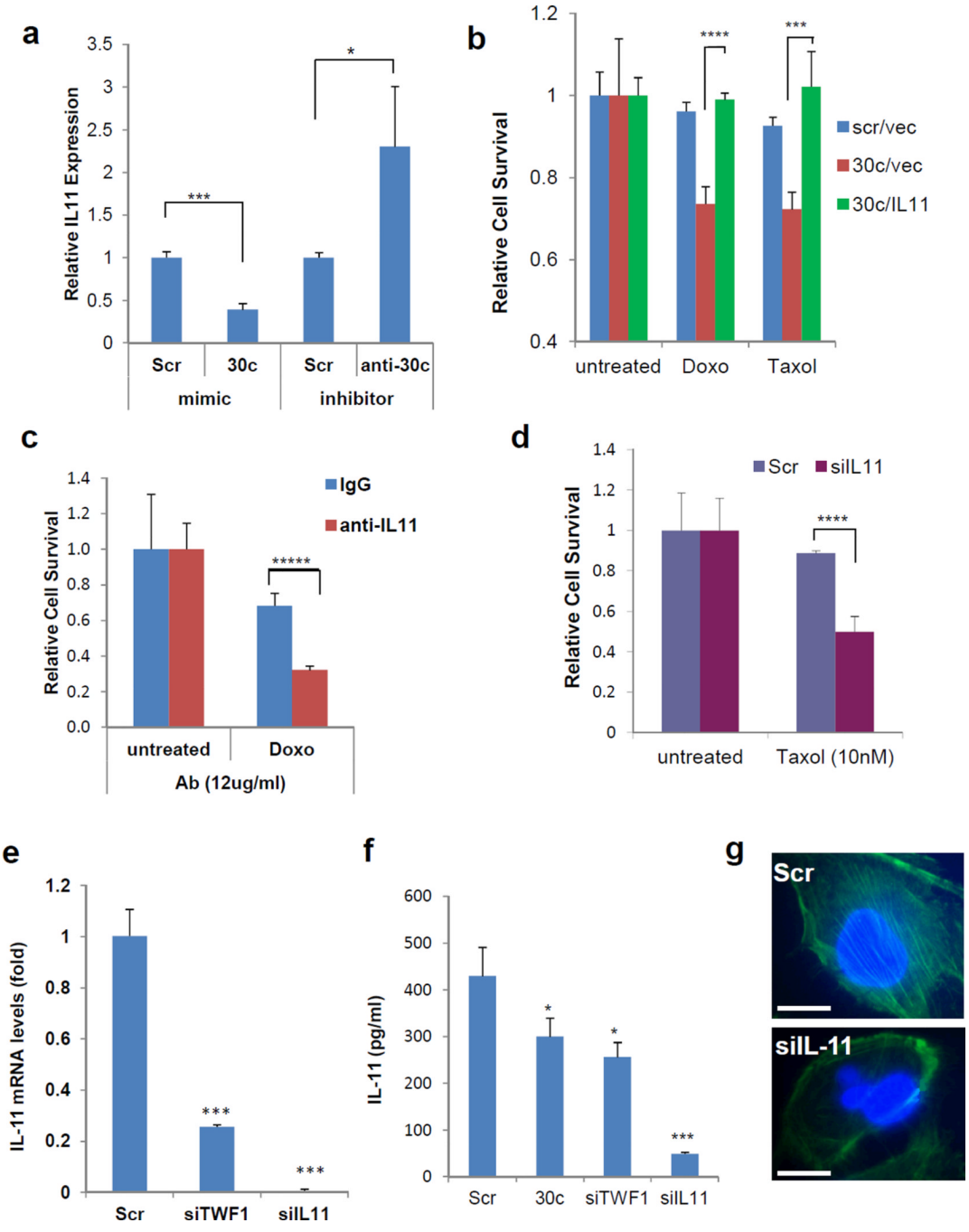

Figure 5. IL-11 as a downstream target of TWF1

a. Relative IL-11 expression levels measured by real-time PCR analyses. The miR-30c oligos (mimic) downregulated IL-11 expression whereas the anti-miR-30c inhibitor upregulated IL-11 expression in MDA-MB-231 cells after 36hrs of transfections, compared to the scrambled control (Scr). *p=0.03299, ***p=0.00052 (n=3) by a T test. Error bars: SD.

b. Overexpression of IL-11 reversed miR-30c–mediated sensitivity of MDA-MD-231 cells to doxorubicin (Doxo) and paclitaxel (Taxol) (n=6). T test p=2.8E-05 (Doxo) and 1.1E-04 (Taxol), when comparing 30c/vector to 30c/IL-11. Error bars: SD.

c. Survival of MDA-MB-231 cells incubated with the goat IgG control or a neutralizing antibody to human IL-11 (12 μg/ml), upon 72-hr exposure to 100nM doxorubicin (Doxo). *****p=4.24E-06 by a T test (n=6). Error bars: SD.
d. Knockdown of IL-11 by siRNAs sensitized cytotoxicity of MDA-MB-231 cells to 72-hour treatment of paclitaxel (Taxol, 10nM). ****p=3.0E-05 by T test (n=6). Error bars: SD.
e. Reduction of IL-11 mRNA expression upon gene knockdowns of siTWF1 and siIL-11, compared to the scrambled control (Scr) (n=3), measured by real-time PCR. ***p=0.0009 (siTWF1) and 0.0003 (siIL-11) by a T test. Error bars: SD.
f. IL-11 levels detected in the cultured media of MDA-231 cells, upon transfections with scrambled, miR-30c, and siRNAs for TWF1 or IL-11 (n=4). T test p=0.0381 (30c), 0.0329 (siTWF1), 0.0007 (siIL11) compared to the scrambled control (Scr). Error bars: SD.
g. Images of F-actin staining of MDA-MB-231 cells, transfected with siRNAs of IL-11 and scrambled control (Scr) (1000x, green for F-actin staining and blue for DAPI staining), white scale bars=5μm. Cells were harvested 36hrs after transfections.

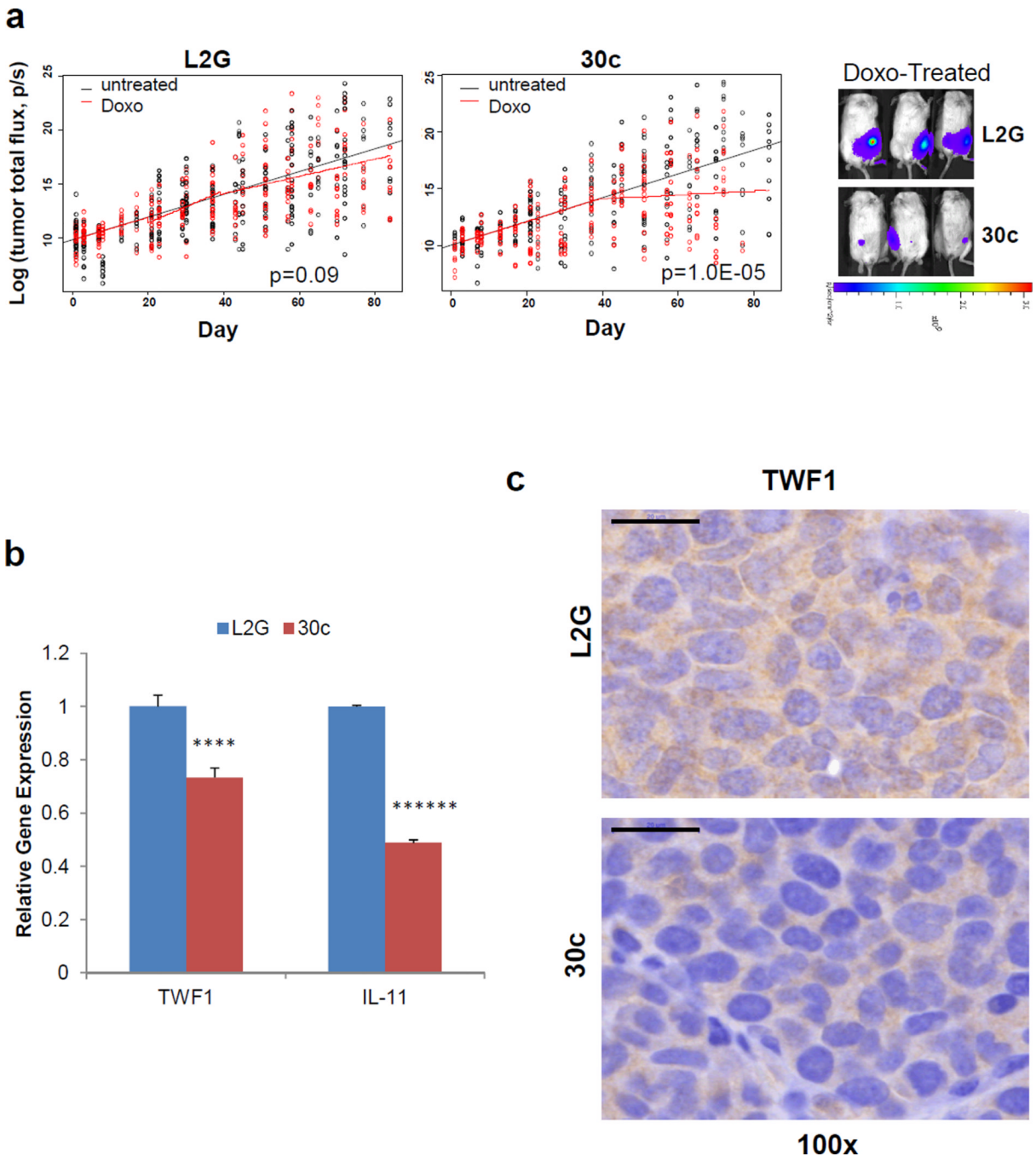

Figure 6. miR-30c regulates chemo-resistance of breast tumour in vivo

a. Doxorubicin treatment response (log-transformed bioluminescence signals) of implanted CD44^{+} human breast tumour cells expressing L2G vector control (left panel, n=40) and miR-30c (middle panel, n=40). The right panel pictures are representative bioluminescence images of treated mice: L2G control (top) and 30c–overexpressed (bottom). Doxorubicin (or PBS vehicle control for untreated) was given intraperitoneally at 1mg/kg to treated mice on day 20 and day 39. In the vector control mice (top panel), doxorubicin (red) did not significantly inhibit tumour growth (slope change after treatment p>0.05, R statistical package analysis) compared to the untreated group (black). In the miR-30c precursor

overexpression group (bottom panel), doxorubicin (red) inhibited tumour growth (slope change p values shown, R model analysis).

b. TWF1 and IL-11 mRNA levels inhibited by pFU-PGK-L2G mediated miR-30c precursor expression in xenograft breast tumour cells (sorted from human-in-mouse tumors *in vivo*), measured by real-time PCR. T test p=0.0001 (TWF1) and 1.04E-07 (IL-11) (n=3). Error bars: SD.

c. Reduced immunohistochemistry staining against human TWF1 in one of three representative 30c–overexpressing primary breast tumour sections, compared to L2G–vector-transduced tumour sections (100x). Scale bars=20μm in both images.

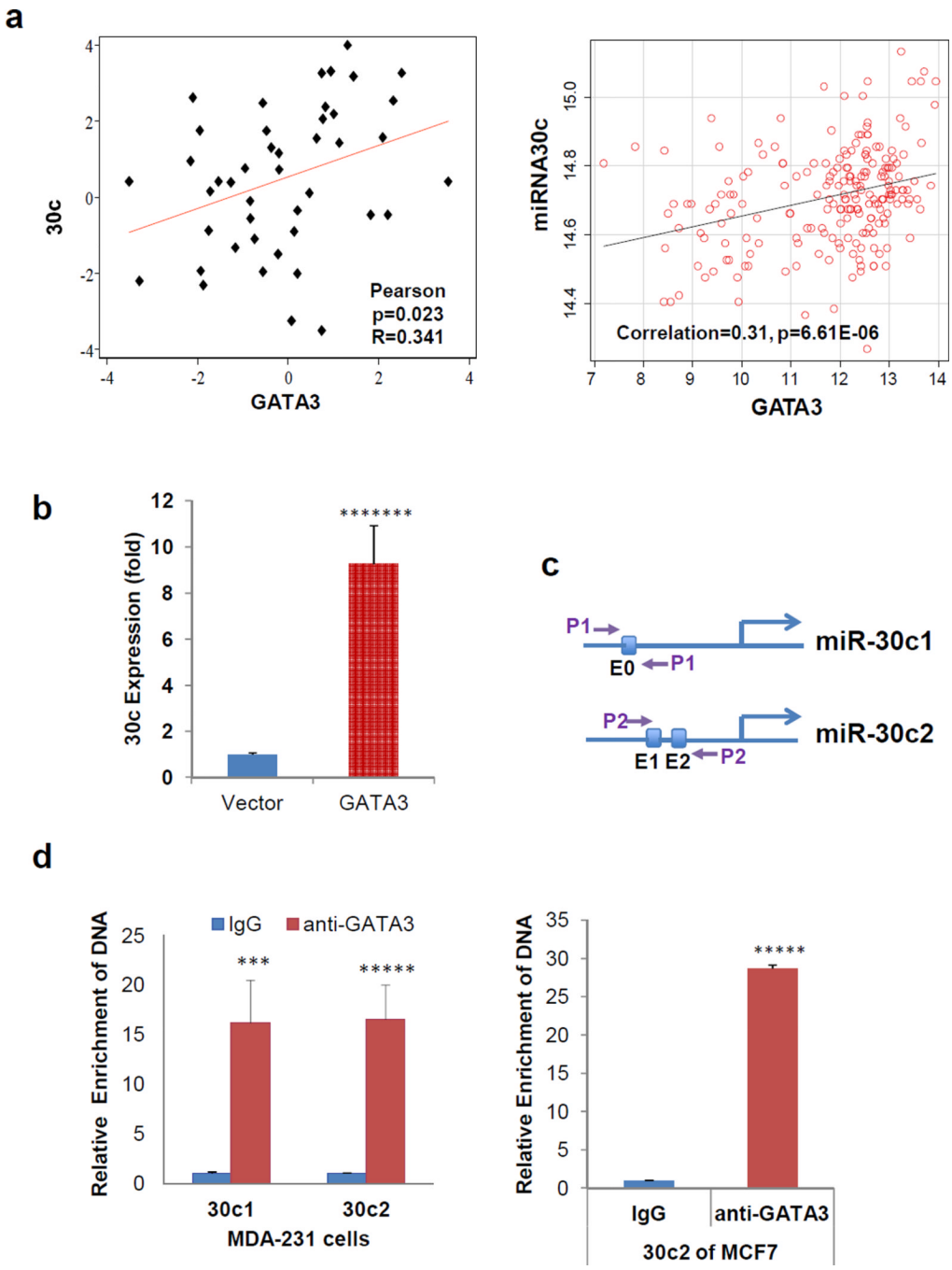

Figure 7. GATA3 regulation of miR-30c

a. Scatter plots of GATA3 expression and miR-30c levels in UC set breast tumors (n=44, p=0.023, R=0.341) (left panel) and Oxford breast tumour sets (GSE22220 and GSE22216) (n=210, p=0.0005, Pearson correlation=0.31) (right panel). Linear regression analyses were performed between miRNA expression and GATA3 levels after log 2 transformation. Plots were drawn using the scatterplot function found in the Car package (http://cran.r-project.org).

b. Induced expression of miR-30c (T test p=1.95E-08, n=5) by ectopic GATA3 in MDA-MB-231 breast cancer cells, measured by real-time PCR, compare to the vector control. Error bars: SD.

c. −3kb promoter regions of hsa-miR-30c1 and 30c2 with predicted GATA3 binding elements (E0 for 30c1, E1 and E2 for 30c2). PCR primers were designed to amplify the regions flanking E0 (P1) or both E1 and E2 (P2).

d. Left panel: the miR-30c promoter regions of 30c1 and 30c2 enriched by GATA3 antibody-mediated chromatin-immunoprecipitation (ChIP) with GATA3-overexpressing MDA-MB-231 lysates, detected by real-time PCR using primers P1 and P2 respectively. Right panel: the miR-30c2 promoter enriched by GATA3 antibody-mediated ChIP with MCF-7, detected by real-time PCR with P2 primers. T test p= 0.0004 (30c1) and 3.59E-06 (30c2) for MDA-MB-231 cells, and 5.23E-06 (30c2) for MCF-7 cells respectively (n=6). Error bars: SD.

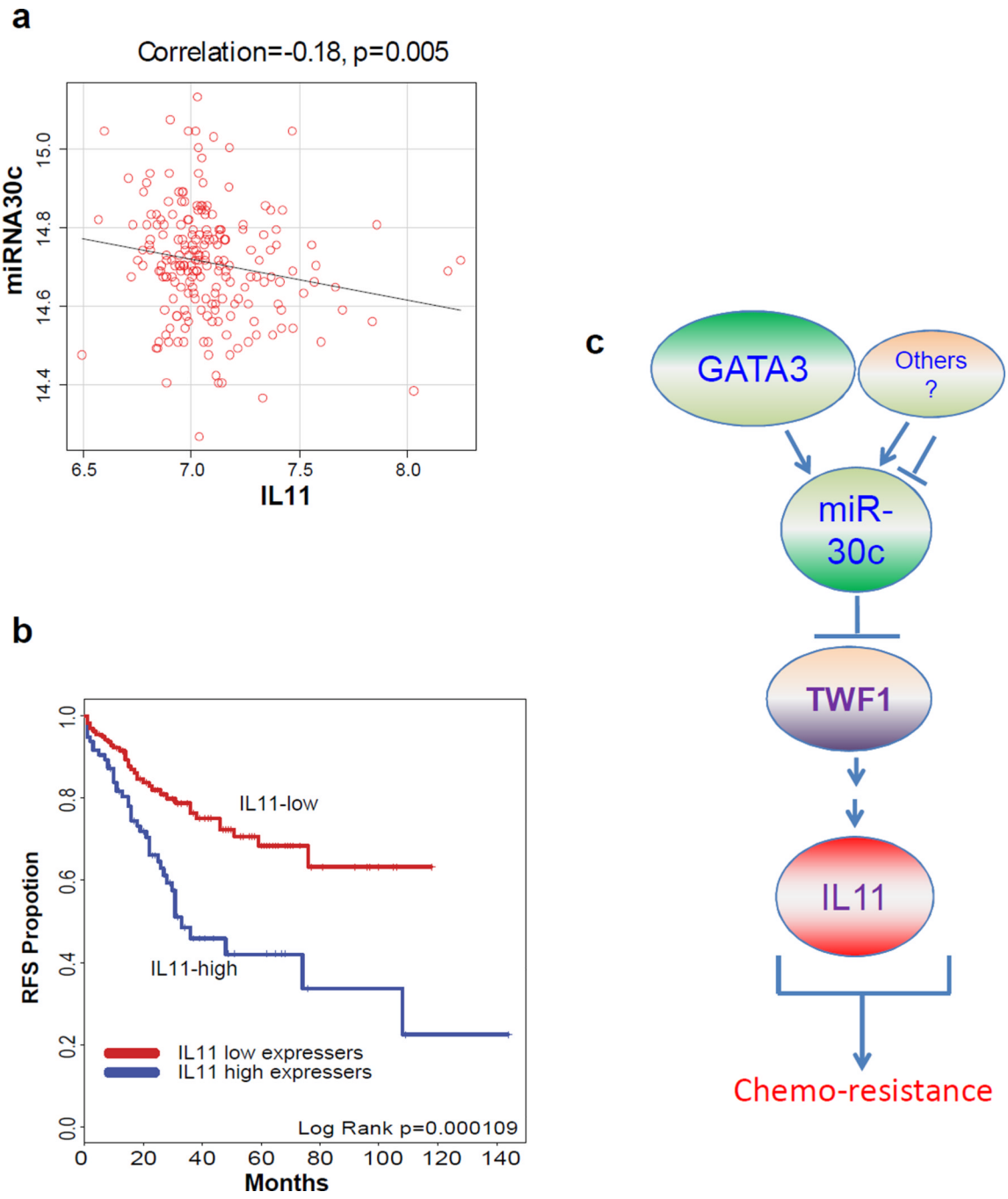

Figure 8. Clinical relevance of the miR-30c signalling pathway

a. Scatter plots between IL-11 single gene expression and the expression of miR-30c in breast cancer dataset with combined expression profiles of mRNA GSE22220 and miRNA GSE22216 (n=210). Pearson correlation was estimated (p=0.005).

b. Survival outcomes of IL-11 gene expression in primary breast cancers in the UNC337 publicly available microarray data set [8]. Relapse-free survival KM plots were based on IL-11 gene expression and median gene expression was used to define low and high expressers (p=0.000109, n=337).

c. Signalling pathway scheme GATA3-miR30-TWF1-IL-11 regulation of breast cancer chemo-resistance.